Journal of *Marine Science and Engineering*

MDPI

Article

Numerical Investigation on Performance Optimization of Offshore Sandwich Blast Walls with Different Honeycomb Cores Subjected to Blast Loading

Hong Lin [1,2,*], Chang Han [1], Lei Yang [3,*], Lin Zhang [4], Haochen Luan [1], Pingping Han [1], Hao Xu [1] and Shuo Zhang [1]

[1] College of Pipeline and Civil Engineering, China University of Petroleum (East China), Qingdao 266580, China
[2] Center for Offshore Engineering and Safety Technology (COEST), China University of Petroleum (East China), Qingdao 266580, China
[3] College of Science, China University of Petroleum (East China), Qingdao 266580, China
[4] CNOOC (Guangdong) Safety & Health Technology Co., Ltd., Zhanjiang 524057, China
* Correspondence: linhong@upc.edu.cn (H.L.); yanglei1021@upc.edu.cn (L.Y.)

Abstract: As an important protective facility on offshore platform, the blast wall is of great significance in resisting oil and gas explosions. Honeycomb structures are widely used due to their unique deformation and mechanical properties under dynamic impact loads. The aim of this research is to develop an optimized design for an offshore sandwich blast wall with different honeycomb cores. The uniqueness of this paper is providing the quantitative optimization scheme for topological configurations and unit cell geometric parameters of honeycomb structures according to mass consistency and the proposed synthetic evaluation index of anti-blast performance. By using the numerical simulation software ANSYS/LS-DYNA, the CONWEP algorithm was first validated and then adopted to conduct the dynamical performance analysis of the honeycomb blast wall. For comparison purposes, simulating studies on a series of different blast walls were carried out by considering various influential parameters. According to different criteria, the blast resistance of the sandwich honeycomb structures was evaluated. It is found that the sandwich plate with concave arc honeycomb core has the best anti-blast performance compared to that of arrow honeycomb core and concave hexagonal honeycomb core. For the concave arc honeycomb structure, the geometric parameters such as concave angle and aspect ratio of honeycomb unit cell have great influence on the blast-resistance performance. Moreover, the concave arc honeycomb structure with positive gradient arrangement has better anti-blast performance than the negative one. The curved blast wall with the curvature of 1/20 achieves better anti-blast performance than the flat blast wall.

Keywords: offshore sandwich blast wall; numerical simulation; CONWEP algorithm; anti-blast performance; auxetic honeycomb

Citation: Lin, H.; Han, C.; Yang, L.; Zhang, L.; Luan, H.; Han, P.; Xu, H.; Zhang, S. Numerical Investigation on Performance Optimization of Offshore Sandwich Blast Walls with Different Honeycomb Cores Subjected to Blast Loading. *J. Mar. Sci. Eng.* **2022**, *10*, 1743. https://doi.org/10.3390/jmse10111743

Academic Editor: Alessandro Antonini

Received: 13 October 2022
Accepted: 10 November 2022
Published: 14 November 2022

1. Introduction

During the long-term operation of oil and gas exploration, offshore jacket platforms, as the most important type of offshore facilities, will be confronted with emergencies, such as accidental blasts caused by gas release and hydrocarbon fires [1–5]. Due to the large overpressures, blast accidents may cause damage to the platform structures or the staff, thus leading to huge losses and endangering the safety of human life. Therefore, various explosion-proof measures should be taken to protect key equipment from explosion loads [6,7]. Among these measures are blast walls that can effectively absorb the explosion energy and reflect the explosion pressure wave, which are widely used in offshore platform structures to ensure the safety of the process structure and personnel. They have the advantages of being low in cost, quick to install, and high in strength [8–11].

As a commonly used explosive barrier, the corrugated plate blast wall has been used widely. The studies concerning their structural response and anti-blast performance have been carried out [6–11] by using numerical simulation and experimental methods. Kang et al. [12] simulated the effects of different loads on blast walls through CFD and compared the dynamic responses of blast walls. Syed et al. [13] used nonlinear finite element analysis to present realistic responses to a variety of high-impact pressure loads generated by oil and gas explosions, and compared them with experiments. Su et al. [14] used the finite element software LS-DYNA to simulate the propagation of explosion shock wave and compared it with the test, thus obtaining the propagation law of the shock wave. However, some scholars [10,15,16] pointed out that the impact of explosion load has been underestimated in the actual anti-explosion design process, and thus the existing corrugated plate structure will be confronted with greater risk of failure.

Nowadays, the honeycomb structure, as an excellent anti-impact structure, has been widely used in various industries involving passive protection due to its excellent energy-absorption capacity [17–21]. By combining one honeycomb core layer and two high-strength plates, a sandwich structure can be constructed with both the advantages of stiffness and strength of the thin face-sheet and lightweight flexible core [22,23]. Therefore, it is a good option to design a sandwich blast wall with different honeycomb cores to achieve superior material and structural properties subjected to blast loading.

The hexagonal honeycomb structure is one of the most commonly used honeycomb structures [24]. Recently, auxetic honeycomb structures [25] with a macro negative Poisson's ratio effect, which have better resistance to impact deformation and energy absorption than conventional honeycomb structures, have attracted the attention of many scholars. Li et al. [26] analyzed the in-plane uniaxial and biaxial crushing characteristics of three kinds of honeycomb structures, including regular hexagon, concave hexagon, and the mixture of regular hexagon and concave hexagon. More and more innovative designs of auxetic honeycomb structures have been developed to improve better performances in anti-impact, such as arrowed honeycomb structures [17], concave hexagon structures [19], gradient honeycomb structures [27], and so on. Jin et al. [27] proposed an innovative sandwich structure with auxetic re-entrant cell honeycomb cores, and studied the influence of different arrangements on the dynamic response of the honeycomb sandwich structure. The results show that graded cores and cross arrangement of the honeycomb sandwich can significantly improve the impact resistance of the honeycomb sandwich structure under an explosive load. Alqwasmi et al. [28] studied the behavior of sacrificial sandwich mild steel panels of axially oriented, octagonal, tapered tubular cores subjected to a near-field impulsive blast. Those studies showed the characteristics of different honeycomb structures under impact loading, and will provide guidance for the further study on the sandwich structures with different honeycomb cores.

Experiments and corresponding finite element simulations have been performed by some researchers to investigate the structural response of honeycomb sandwich panels loaded by blasts. An auxetic honeycomb under the close-in detonation test has been carried out by Qi et al. [29], and the corresponding numerical simulation has been done by using a simplified method called the blast impact impulse model (BIIM). Luo et al. [20] used the method of load curve to simulate behavior of corrugated plate blast walls and honeycomb sandwich blast walls under blast loading. Imbalzano et al. [30] conducted numerical simulation by using the CONWEP method on the dynamic performance of sandwich panels composed of honeycomb structures and metal panels with a negative Poisson's ratio under pulse load, and found that the composite panel has better energy-absorption capacity than a single panel. Some researchers have studied the simulation of explosion by using the meshless method, which has the advantages of dealing with large deformation and material fracture [31–34].

As has been discussed, a great deal of work on honeycomb sandwiches under impact loading have been done. Nevertheless, investigations on the quantitative influences of configurations and geometric parameters of the honeycomb structure on the dynamic

performance of the structure is rarely examined [35]. Moreover, to the best of the authors' knowledge, there are few studies on the optimization design of sandwich blast walls on offshore platforms, especially considering the advantages of the superior energy-absorption characteristics of the auxetic honeycomb cores with the curved configuration of the sandwich blast wall. The aim of this research is to provide the quantitative optimization scheme for topological configurations and unit cell geometric parameters of the auxetic honeycomb structure according to mass consistency and the proposed synthetic evaluation index of anti-blast performance, so as to obtain a good result for the offshore blast wall under blast loading. By using the numerical simulation software ANSYS/LS-DYNA, the CONWEP algorithm was first validated and then adopted to conduct the dynamical performance analysis of the honeycomb blast wall. Moreover, the anti-blast resistance of the honeycomb structures is evaluated through different criteria. For comparison purposes, simulating studies on a series of different blast walls are carried out, considering the following effects to obtain the optimal design of the blast wall, including (1) different type of honeycomb cells (namely the arrow type, concave hexagonal type, concave arc type, and gradient honeycomb), (2) different geometric parameters (such as concave angle, aspect ratio, and gradient direction of honeycomb unit cell), and (3) different curvatures of the sandwich blast wall configuration. This study could serve as guidance for performance optimization of offshore sandwich blast walls.

2. Description of the Honeycomb Structure

2.1. Geometric Characteristics of the Sandwich Blast Walls

As stated above, the sandwich blast walls with different honeycomb cores, namely the arrow honeycomb structure, concave hexagonal honeycomb structure, and concave arc honeycomb structure, are constructed. The cross-section of each honeycomb unit cell is shown in Figure 1.

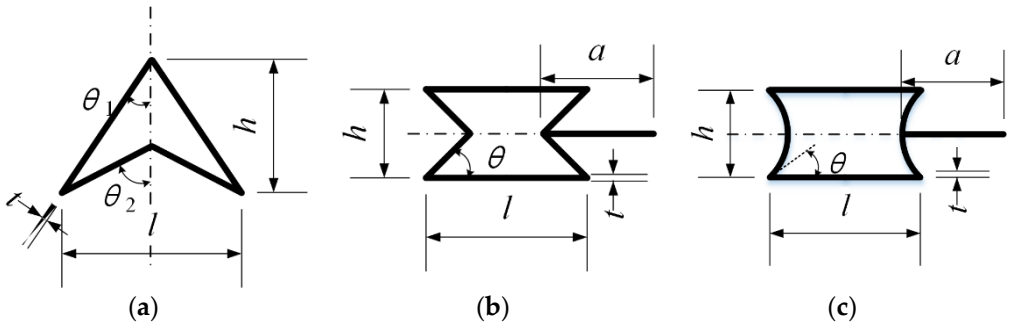

Figure 1. Cross-section of different unit cell. (**a**) Arrow; (**b**) Concave hexagon; and (**c**) Concave arc.

Figure 2 shows the geometrical illustration of the honeycomb core with height of H and thickness of T. In order to ensure the mass consistency of different honeycomb cores, the concept of relative density [36] was used to design the honeycomb cores. Let N_1 and N_2 represent the number of cells along the height direction and thickness direction of the honeycomb structure, respectively. Thus, the relative density of the arrow honeycomb core $\Delta\rho_{\mathrm{A}}$, the relative density of the concave hexagonal honeycomb core $\Delta\rho_{\mathrm{Ch}}$, and the relative density of the concave arc honeycomb core $\Delta\rho_{\mathrm{Ca}}$, are given as follows:

$$\Delta\rho_{\mathrm{A}} = t\frac{(2h/\cos\theta_1 + l/\sin\theta_2)N_1N_2}{HT} \tag{1}$$

$$\Delta\rho_{\mathrm{Ch}} = t\frac{2N_1N_2h/\sin\theta + N_1(N_2+1)l + N_2(N_1-1)a}{HT} \tag{2}$$

$$\Delta\rho_{\mathrm{Ca}} = t\frac{N_1N_2(\pi-2\theta)h/\cos\theta + N_1(N_2+1)l + N_2(N_1-1)a}{HT} \tag{3}$$

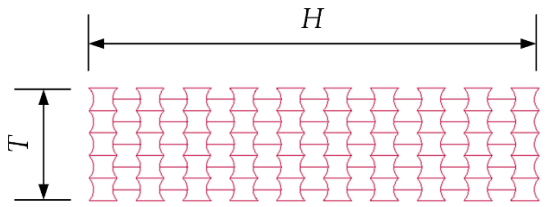

Figure 2. Dimensions of the structure.

Here, for comparison purposes, the relative densities of the three types of honeycomb cores $\Delta\rho_A$, $\Delta\rho_{Ch}$, and $\Delta\rho_{Ca}$ should be equal; accordingly, the numbers of the honeycomb cell and the dimensions of each honeycomb cell can be determined. The cell numbers and dimensions of the three honeycomb cores have been calculated while keeping the relative densities consistent, as listed in Table 1.

Table 1. Dimensions of each unit cell of the honeycomb core.

Type	h (m)	l (m)	θ_1 (°)	θ_2 (°)	N_1	N_2	t (m)	a (m)
Arrow	0.05455	0.06298	30	60	13	5	0.00069	/
Concave hexagonal	0.04	0.05	45		10	5	0.00075	0.07333
Concave arc	0.04	0.05	45		10	5	0.00092	0.04990

2.2. Anti-Blast Index of Honeycomb Structure

Multiple indicators are adopted to understand the anti-blast performance of the honeycomb, such as the maximum deflection (δ_{max}) and specific energy absorption (SEA).

The maximum deflection (δ_{max}) serves as a commonly used index to assess the deformation under blast loading. A smaller δ_{max} generally appears on the sandwich structure of stronger anti-blast performance.

SEA is defined as the amount of energy absorbed per unit mass of a honeycomb structure, which can be defined as

$$SEA = \frac{TEA}{M} \tag{4}$$

$$TEA = \int_0^{\varepsilon} \sigma(\varepsilon) d\varepsilon, \tag{5}$$

where M is the mass of the honeycomb structure, and TEA is the total plastic energy absorption of the honeycomb structure, which can be calculated as in Equation (5).

The higher value of SEA represents the better anti-blast performance of sandwich structures.

As can be seen from the definition of the above two indices δ_{max} and SEA, both the two indices should be considered in the actual anti-blast design of the sandwich blast wall. Here, to give a comprehensive assessment of the anti-blast performance of sandwich structures, the ratio P of SEA to δ_{max} could be defined as follows:

$$P = \frac{SEA}{\delta_{max}}, \tag{6}$$

which indicates the specific energy absorption per unit impact depth of the structure. It can be seen that the higher value of P represents the better anti-blast performance of sandwich structures.

3. Numerical Simulation Method and Verification

3.1. FE Models of the Sandwich Honeycomb Blast Wall

The numerical simulations were conducted by using ANSYS/LS-DYNA software, which is a powerful explicit finite element analysis (FEA) tool. The sandwich blast wall consists of two face plates and five layers of honeycomb cores. Because the sandwich panel is symmetric, only a 1/4 model was established, as shown in Figure 3. The dimension of

the sandwich panel is 1 m × 0.8 m. The thickness of both the face plates is 2 mm, and the thickness of each core structure is 200 mm; thus, the total thickness of the panel is 204 mm.

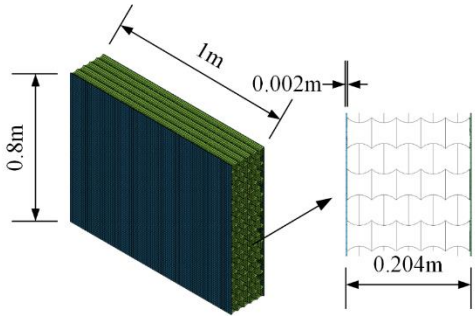

Figure 3. Sandwich blast wall dimensions.

Honeycomb cores were modeled by using SHELL163 element. The thin plates of the sandwich structure were modeled by using SOLID164 element. The interactions between the face plates and cores were defined as *CONTACT_TIED_SHELL_EDGE_TO_SOLID.

Due to the large difference between the size of honeycomb unit cell and the face plate, the size of the grids will have significant influences on the simulation results. After grid sensitivity analysis, the grid size is defined as 0.01 m, which will both ensure the accuracy and efficiency of the calculation. Figure 4 shows the FE models of the three sandwich panels with different configuration of honeycomb core.

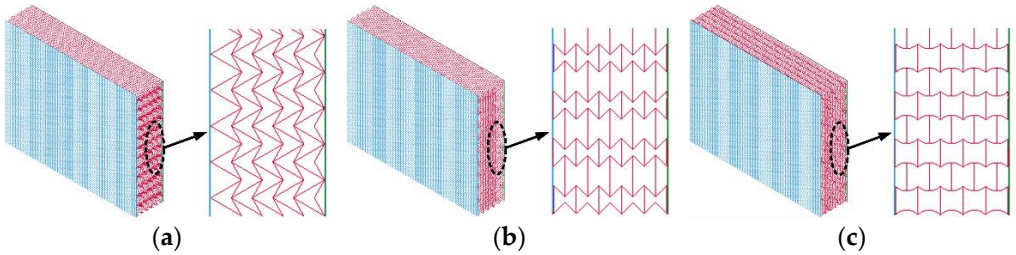

Figure 4. The FE model of sandwich panel. (**a**) configuration I, Arrow-shape; (**b**) configuration II, Concave hexagon-shaped; and (**c**) configuration III, Concave arc-shaped.

3.2. Material Model

During the explosion process, huge explosion shock waves usually lead to plastic deformation or even fracture of the material. Therefore, it is essential to resolve the proper material modeling. In this study, the 316 stainless steel is selected as the material of face-sheets, and the three types of honeycomb cores are made of A5052 aluminum.

The strain rate is directly related to the yield limit of the material and has an important influence on the simulation results. Here, the Cowper–Symonds constitutive model (Cowper et al., 1957 [37]; Storheim et al., 2015 [38]) is used to describe the plastic strain hardening of 316 stainless steel [39] and A5052 aluminum [40], which can reflect strain rate effect as follows:

$$\sigma_y = \left[1 + \left(\frac{\dot{\varepsilon}}{C}\right)^{\frac{1}{P}}\right]\left(\sigma_0 + E_p \varepsilon_p^{eff}\right) \tag{7}$$

$$E_p = \frac{E_{\tan} E}{E - E_{\tan}}, \tag{8}$$

where σ_0 is the initial yield stress, $\dot{\varepsilon}$ is the strain rate, ε_p^{eff} is the effective plastic strain, E_P is the plastic hardening modulus, and C and P are the strain rate parameters, respectively.

In the simulations, the mechanical behaviors of 316 stainless steel and A5052 aluminum were modeled with material type 3 (*MAT_PLASTIC_KINEMATIC) in LS-DYNA, which is a bilinear elastic–plastic constitutive relationship that contains formulations incorporating

isotropic and kinetic hardening. The material attributes and parameters of the two material models are given in Table 2.

Table 2. Material attributes of 316 stainless steel and aluminum A5052.

Material Attributes	316 Stainless Steel	Aluminum A5052
density (ρ) (kg/m^3)	7850	2700
elastic modulus (E) (GPa)	210	62
Poisson's ratio (ν)	0.3	0.3
yield stress(σ_0) (MPa)	353.7	225
tangent modulus(E_{tan}) (GPa)	3.6	50
Strain rate parameter (P)	5.2	4
Strain rate parameter (C)	1704.5	6000

3.3. Blast Loading and Boundary Setting

In the existing research, different methods are adopted to simulate explosions, including the arbitrary Lagrangian–Eulerian (ALE) algorithm, the CONWEP algorithm, the coupling algorithm, and the pressure–time history curve method [41,42]. Nevertheless, the pressure–time history curve method is a simplified method that is unable to give good results to the real blast wave load. Moreover, both the ALE and coupling algorithms require the establishment of large air domains containing structures that will result in huge computational efforts. Therefore, in this paper, the CONWEP method was used to conduct numerical simulation due to its advantage of keeping a balance between computational accuracy and computational effort.

The equivalent TNT method was adopted with the explosive equivalent defined as 100 kg and the start time of explosion set as 0 s by using the keyword *LOAD_BLAST. Moreover, the keyword *LOAD_SEGMENT_SET was used to apply the explosion load to the explosion surface. In the simulations, the explosive was detonated in front of the centre of the structures with a distance of 5 m, as shown in Figure 5.

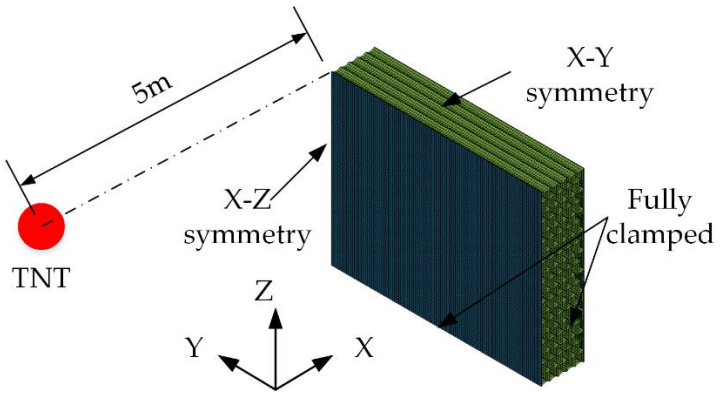

Figure 5. Diagram of TNT position and boundary conditions.

Because the sandwich panel is symmetric about the X-Z and Y-Z planes, a fully clamped boundary condition was prescribed on the perimeter of the plate.

3.4. Verification of CONWEP Method

First, in order to verify the correctness and accuracy of the CONWEP method in calculating the peak overpressure during blast, the empirical formulas were used for comparison. According to [43], the peak overpressure P_m could be calculated as follows:

$$P_m = 10^{\alpha}/145 \quad (9)$$

$$\begin{aligned}\alpha = {} & 2.391 - 2.214U + 0.0351U^2 + 0.658U^3 \\ & +0.0142U^4 - 0.243U^5 - 0.0159U^6 \\ & +0.0493U^7 + 0.00228U^8 - 0.00397U^9\end{aligned} \tag{10}$$

$$U = -0.757 + 1.35\lg(2.52Z) \tag{11}$$

$$Z = R/W^{1/3} \tag{12}$$

where P_m is the peak overpressure, Z is the ratio of distance, R is the distance between the explosive and the plate, and W is the equivalent mass of TNT.

According to the empirical formulas, the peak overpressure of this verified experiment was calculated and listed in Table 3. By comparing the value of the peak overpressure obtained from the CONWEP method and the empirical formulas, it can be found that the two results are very close, with an error of only 0.29%. This proves that the CONWEP method adopted in this paper has high computational accuracy.

Table 3. Comparison of peak overpressure.

	CONWEP Method	Empirical Formula	Error
Peak overpressure	279.419 MPa	278.604 MPa	0.29%

Next, the CONWEP method was used for the verification simulation of a clamped circular steel plate under blast loading, which is consistent with the research made by Neuberger [44] and compared with both the explosion test results [44] and the FE simulation results of Ni [45], as shown in Figure 6.

(**a**) (**b**)

Figure 6. (**a**) Diagram of the validated test of Neuberger [44]. (**b**) Simulated deformation of [45].

In Neuberger' test [44], a circular steel plate with a diameter of 1 m and a thickness of 0.02 m was designed to be subjected to an equivalent TNT of 3.75 kg, and the distance between the explosive and the circular steel plate is 0.2 m. All sides of the circular steel plate are fully fixed constraints.

Here, the verification model of this study, consistent with [44], are established by using SHELL163 element in ANSYS/LS-DYNA. The same material parameters of the simplified Johnson–Cook constitutive model are adopted, which are consistent with [44], as shown in Table 4.

Table 4. Material properties of simplified Johnson–Cook constitutive model.

Properties	ρ (kg/m^3)	E (GPa)	ν	A (MPa)	B (MPa)	n	c
Value	7830	210	0.28	950	560	0.26	0.014

Figure 7 shows verification FE model and the simulated deformation of this study. It can be seen that the verification results are consistent with both the experiment results and simulation results of [45]. Furthermore, the time–history curve of central deflection of the circular plate were drawn in Figure 8, so as to give a detailed comparison between the verification results with the simulation of [45]. In addition, the maximum value of

the center deflection of the circular steel plate is listed in Table 5 and is compared with the test results of [44] and simulation of [45]. It could be found that the results obtained in this paper is 53.75 mm, which is closer to the test results of 54.0 mm with the error of 0.46%. From the verification, it can be concluded that the CONWEP method has high computational accuracy, which is feasible for the simulation of the blast.

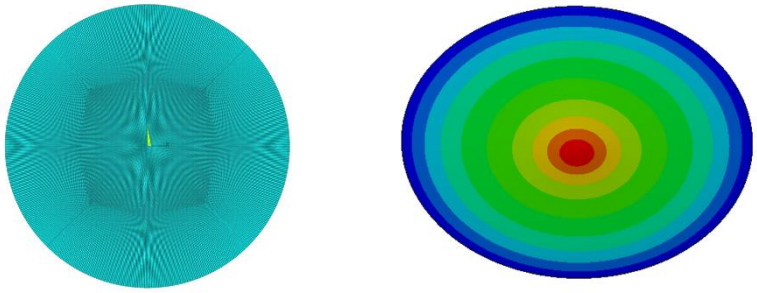

(**a**) (**b**)

Figure 7. Verification of this study. (**a**) FE model; and (**b**) simulated deformation.

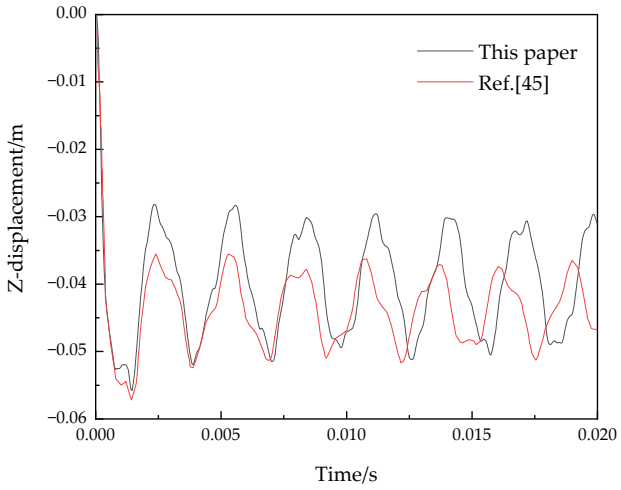

Figure 8. The central displacement time–history curve of circular plate.

Table 5. Comparison of center deflection results.

	Results of Ref. [44]	Results of Ref. [45]	Results of This Study
The center deflection	54.00 mm	57.32 mm	53.75 mm
Error	\	6.15%	0.46%

4. Simulation Results of Different Sandwich Blast Walls

4.1. Deformation Mode Comparison of Different Sandwich Blast Walls

To investigate the deformation modes of different sandwich structures under blast loading, numerical simulations were performed on three kinds of honeycomb cores and the results were compared.

Typical deformation modes of the sandwich panel with an arrow honeycomb core (configuration I), a concave hexagonal honeycomb core (configuration II), and a concave arc-shaped honeycomb core (configuration III), is shown in Figure 9a–c, respectively. By comparing the deformation of the three kinds of configurations, it can be found that although the deformation range of configuration III is larger than that of the other two kinds, the maximum deflection is smaller than that of the other two kinds.

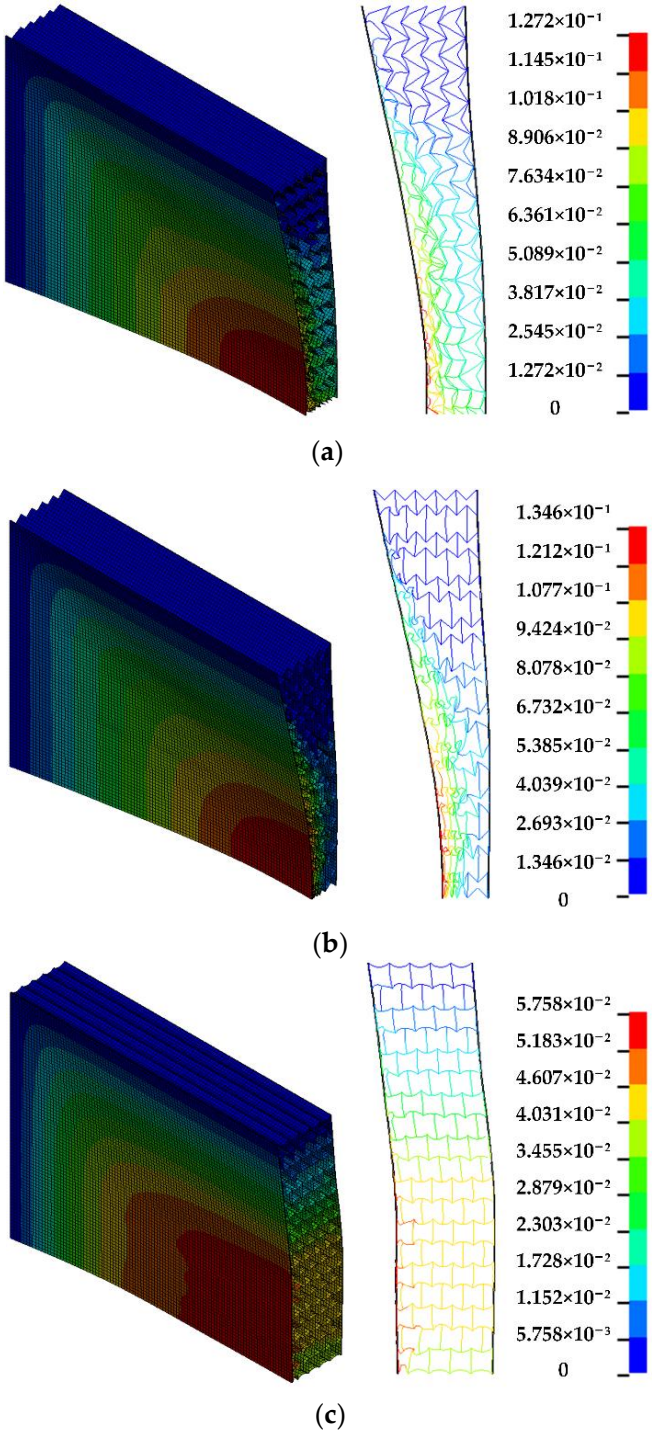

Figure 9. Deformation of sandwich panel with different honeycomb core. (**a**) arrow honeycomb structure; (**b**) concave hexagonal honeycomb structure; and (**c**) concave arc-shaped honeycomb structure.

The cross-section views of the deformation contour of three configurations show that two different deformation modes appear on the three configurations. The "center dishing deformation" appears on configuration I and configuration II due to their more concentrated compression deformation around the center of the structure; thus, it could be regarded as a compress-dominated deformation. Parallelogram bending appears in configuration III because its deformation is more uniformly distributed in the whole structure, which could be regarded as a bending-dominated deformation.

4.2. Assessment of Anti-Blast Resistance of Different Blast Walls

The maximum deflection δ_{max} was defined as the deflection of the central points of the front face plate, which is the biggest in the whole sandwich structure. The values of δ_{max} of the three configurations have been calculated and listed in Table 6. By comparing the δ_{max}, it can be seen that the sandwich plate with concave arc honeycomb (configuration III) has the smallest deformation of 0.0575835 m, whereas the sandwich plate with concave hexagon honeycomb (configuration II) has the biggest deformation of 0.1346310 m. From this viewpoint, the result demonstrates that the sandwich plate with concave arc honeycomb (configuration III) has the best performance to resistant deformation caused by blast loading.

Table 6. Anti-blast indices of the three configurations.

Configuration	δ_{max} (m)	*SEA* (J/kg)	*P* (J/(kg·m))
I (Arrow)	0.1272280	1363.178882	10,714.45658
II (Concave hexagon)	0.1346310	1516.538976	11,264.41144
III (Concave arc)	0.0575835	1138.625587	19,773.46961

On the other hand, the anti-blast resistance of the blast wall could be evaluated from the *SEA* of the sandwich structure. The values of *SEA* of three configurations have been calculated and listed in Table 6. By comparing the *SEA*, it can be seen that the concave arc honeycomb (configuration III) has the smallest *SEA* of 1138.625587 J/kg, whereas the concave hexagon honeycomb (configuration II) has the biggest *SEA* of 1516.538976 J/kg. From this viewpoint, the result demonstrates that the concave hexagon honeycomb (configuration II) has the best energy absorption ability during blast process, which seems to be inconsistent with the evaluation based on the index of maximum deformation δ_{max}.

As stated above in Section 2.2, the comprehensive index of ratio *P* could serve as the good option to evaluate the anti-blast performance of the sandwich blast wall. Thus, the values of *P* have been calculated and listed in Table 6. Comparing the three indices in Figure 10, it can be seen that the sandwich panel with the concave arc honeycomb core (configuration III) has the biggest *P* of 19,773.46961 J/kg·m, which proves that configuration III could provide the best protection to the equipment under blast loading among the three types of honeycomb structures.

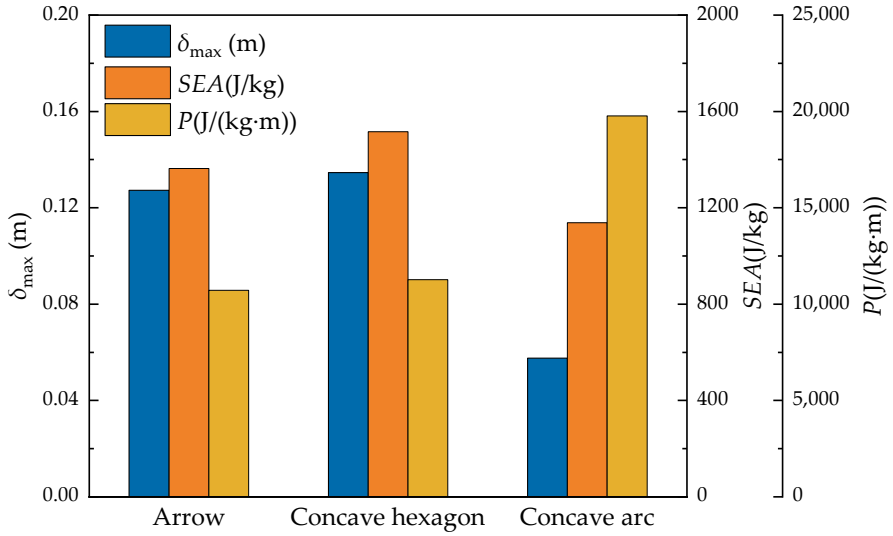

Figure 10. Anti-blast indices of three honeycomb structures.

4.3. Deformation Mechanism of Concave Arc Honeycomb

In order to give a detailed deflection histories of the sandwich plate with concave arc honeycomb (configuration III) structure during the blast loading, three positions, namely

front face plate, back face plate, and honeycomb core, were selected to monitor their deflections, and the corresponding cures were plotted in Figure 11. It can be seen that the biggest deflection appears on the center of front face plate, whereas the back face plate has a smaller deflection. The honeycomb core crushing length, which is defined as the difference between the central points of the two face plates, has the smallest values.

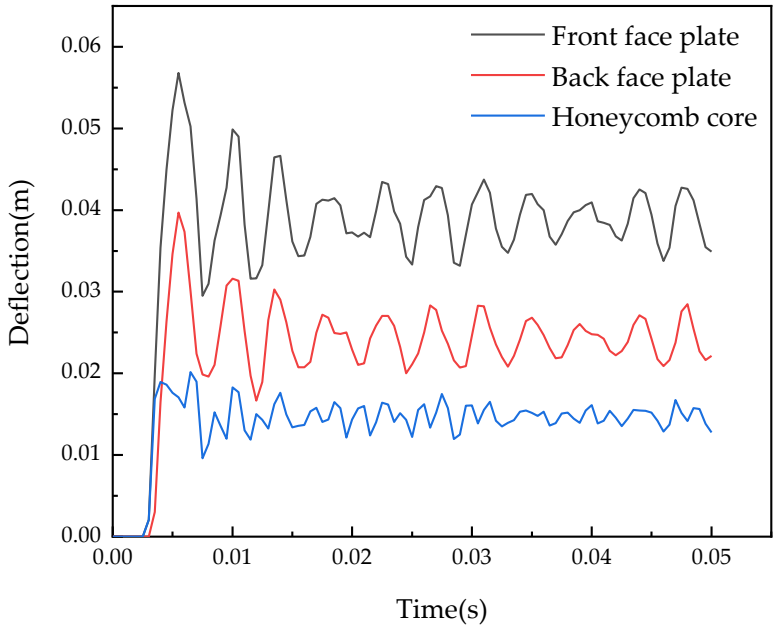

Figure 11. Deflection histories of the concave arc honeycomb.

In order to understand the deformation mechanism of the concave arc honeycomb better, displacement distribution along the X direction caused by plastic deformation was studied. For comparison purposes, five points located at each layer were selected as shown in Figure 12, and the displacement along the X direction was plotted in Figure 13. It could be found that uniform deformation appears on most of the points along the X direction except for the only point located on the front face plate. This uniformly distributed deformation of configuration III will provide better protection to the body subjected to blast loads.

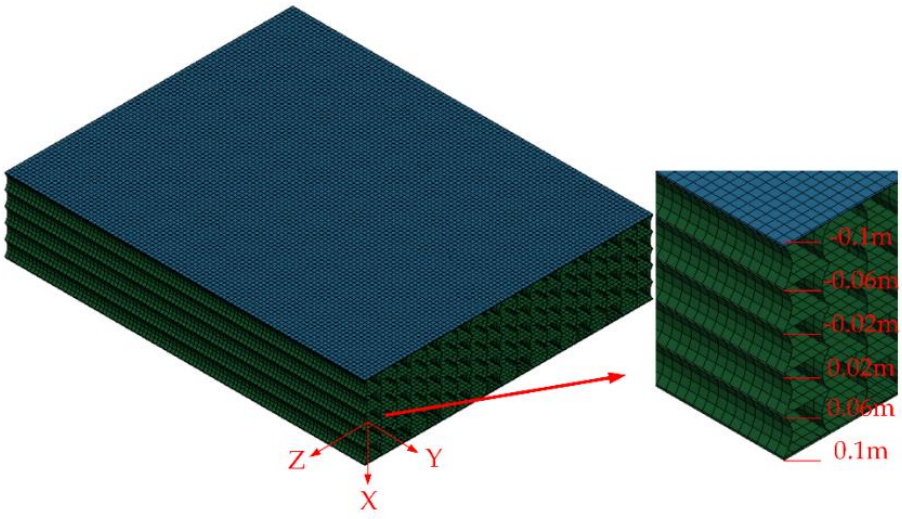

Figure 12. Illustration of the points along the X direction of the concave arc honeycomb.

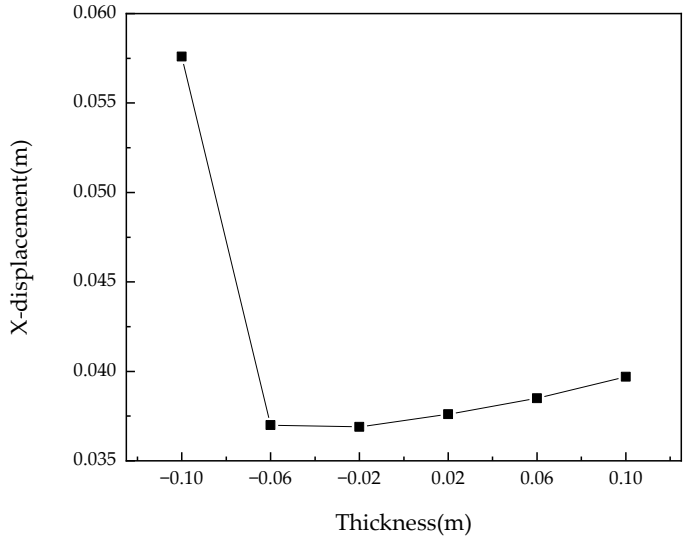

Figure 13. Displacement of the points along the X direction of the concave arc honeycomb.

5. Optimization for Anti-Blast Performance of Concave Arc Honeycomb Structure

5.1. Optimization Parameters Seletion

From the analysis results and assessment results presented above in Sections 4.1 and 4.2, it has been proven that the concave arc honeycomb core could be selected as the fundamental configuration to be constructed for the sandwich blast wall. However, as is known, different geometric parameters of the honeycomb unit cell, such as concave angle (θ) and aspect ratio (l/h), will also play important roles on the performance when submitted to blast loading.

Moreover, the graded honeycombs, consisting of gradient cells with interesting mechanical properties, have attracted much attention [46]. The mechanical properties could be altered by altering the geometric parameters of the honeycomb unit cell. It has been proven that for the honeycomb structure, the gradient arrangement along the impact direction has a great impact on the in-plane impact resistance of the honeycomb material. Therefore, in the following section, honeycomb structure with different gradient assessment direction will be checked for better explosion resistance.

Thus, after we have selected the concave arc honeycomb core as the fundamental configuration, the next step is to optimize the different geometric parameters, so as to obtain the best anti-blast performance.

5.2. Optimization of Concave Arc Honeycomb

5.2.1. Optimization of Concave Angles

Seven concave angles (θ) including 15°, 25°, 35°, 45°, 55°, 65°, and 75°, have been chosen to design the concave arc honeycomb core, whereas other parameters should be kept consistent when changing the concave angle.

Figure 14 shows the established FE model of the concave arc honeycomb sandwich structures with different concave angles. Numerical analysis of these models has been carried out based on the same simulation method.

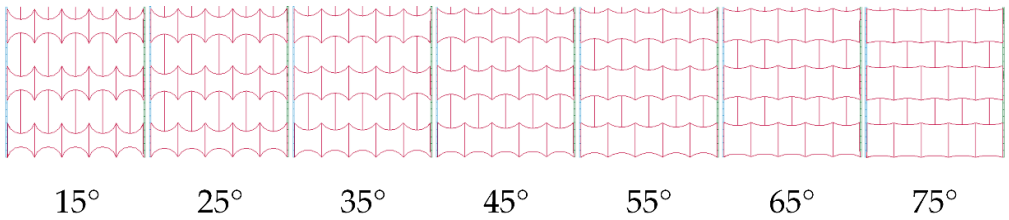

Figure 14. Concave arc honeycomb with different concave angles.

The contours of the deflection (δ_{max}) of the sandwich structures with different concave angles (θ) were shown in Figure 15. It can be seen that the deformation could be classified into two types of deformation modes; specifically, center dishing appears when θ is smaller than 35°, and parallelogram bending appears when θ is bigger than 45°.

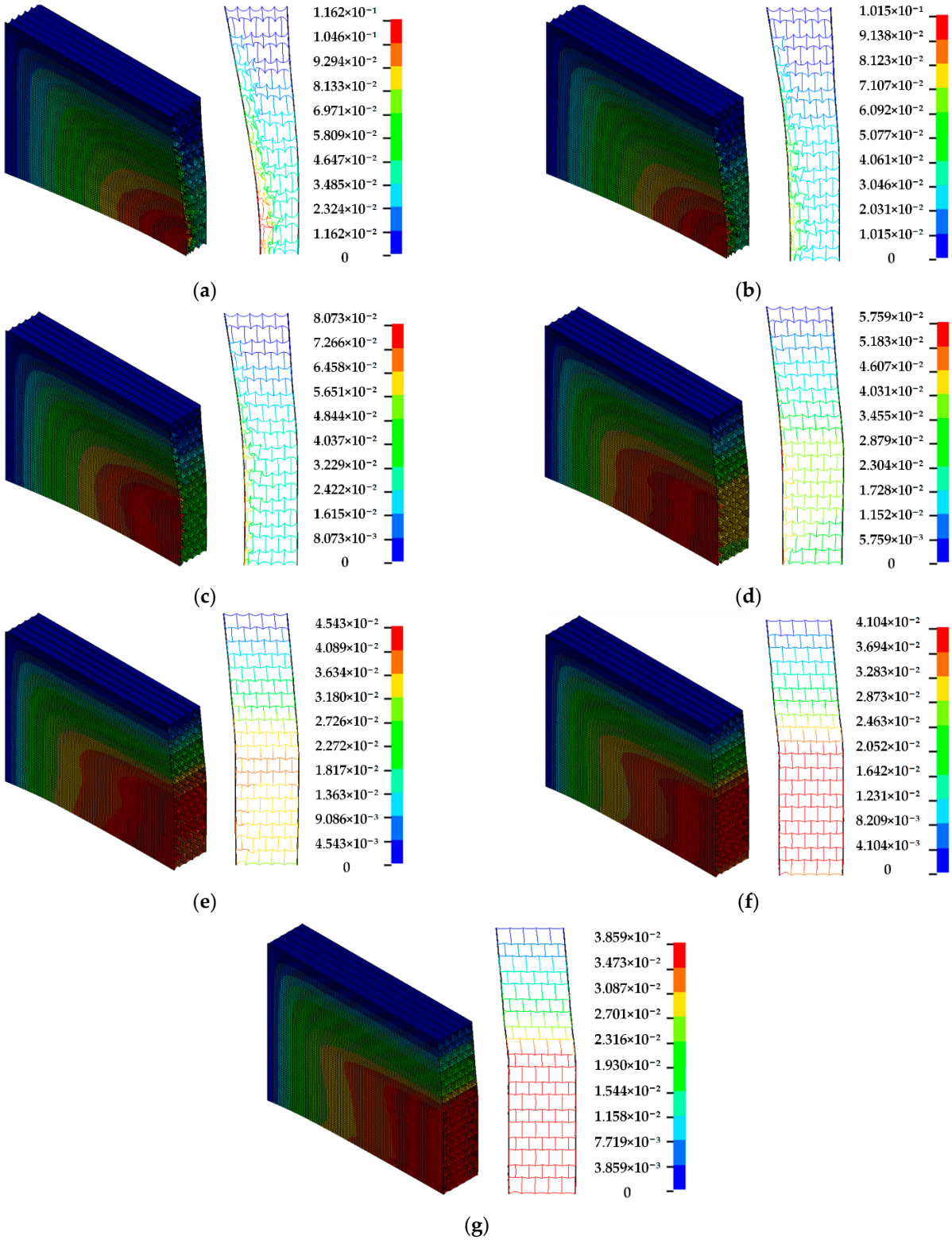

Figure 15. Deformation of different concave angles. (**a**) 15°; (**b**) 25°; (**c**) 35°; (**d**) 45°; (**e**) 55°; (**f**) 65°; (**g**) 75°.

Figure 16a shows δ_{max}-θ curve, from which it can be seen that the maximum deflection δ_{max} of the sandwich honeycomb structure gradually decreases with the increase of the concave angle θ. The results show that the bigger the θ is, the better performance can be obtained to reduce the amount of the maximum deformation.

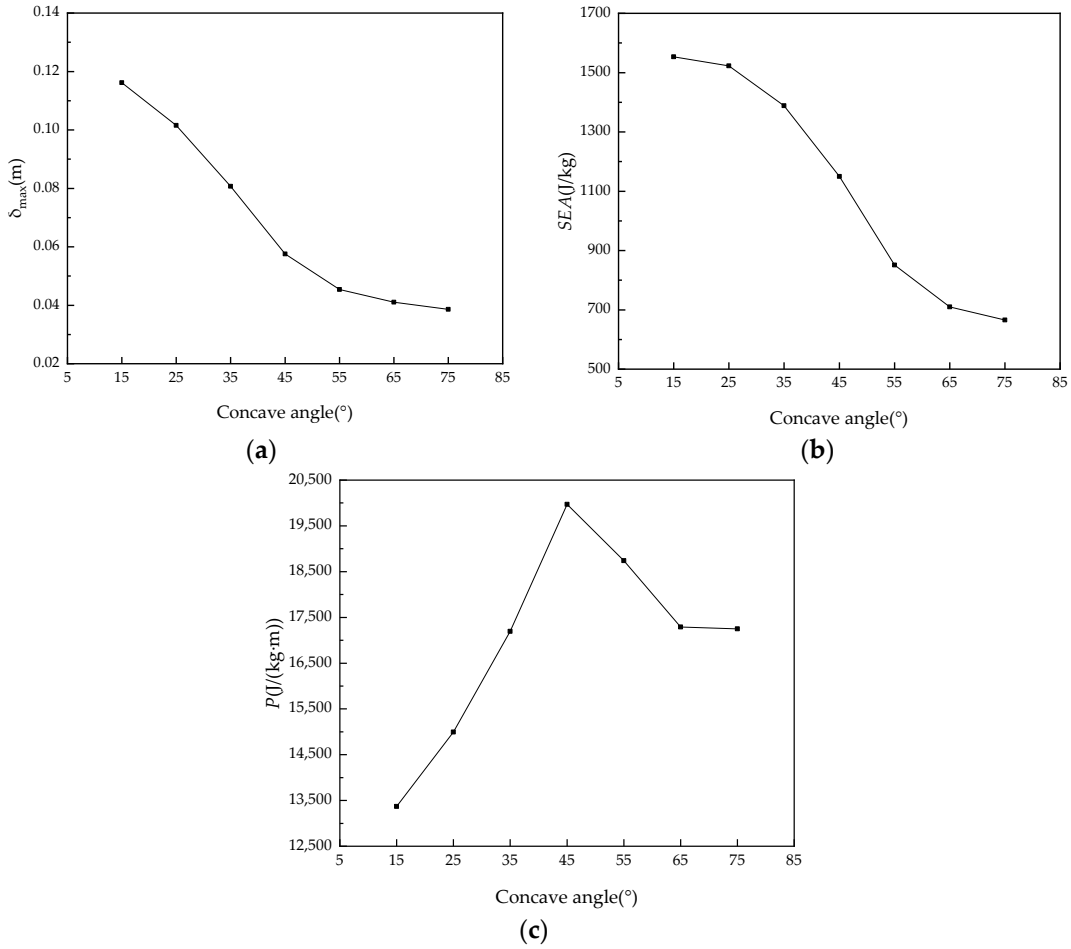

Figure 16. The curves of anti-blast indices of different concave angle. (**a**) $\delta_{\max}$-θ curve; (**b**) *SEA*-θ curve; and (**c**) *P*-θ curve.

Figure 16b shows the *SEA*-θ curve, from which it can be seen that the *SEA* of the sandwich honeycomb structure gradually decreases with the increase of θ. The results show that the smaller the concave angle is, the better performance can be obtained to absorb more energy produced by the blast.

Moreover, the ratio (P)- concave angle (θ) curve has been plotted and shown in Figure 16c, from which it could be seen that with the increase of θ, the ratio P increases at first and then decreases. When θ is 45°, the ratio p reaches the maximum. It can be seen from Figure 14 that when θ increases, the arc becomes more and more straight. When the concave angle is large enough, the concave arc structure itself will lose the characteristic of negative Poisson's ratio and the advantage of energy absorption, so that the value of P will be reduced.

5.2.2. Optimization of Aspect Ratio of Concave Arc Honeycomb Structure

Figure 17 shows the concave arc honeycomb structure model with 6 aspect ratio (l/h) including 1.0, 1.1, 1.2, 1.3, 1.4, and 1.5.

The deformation contours of the sandwich honeycomb structures with different aspect ratios are plotted in Figure 18. It can be seen that only one deformation mode (i.e., parallelogram bending) appears.

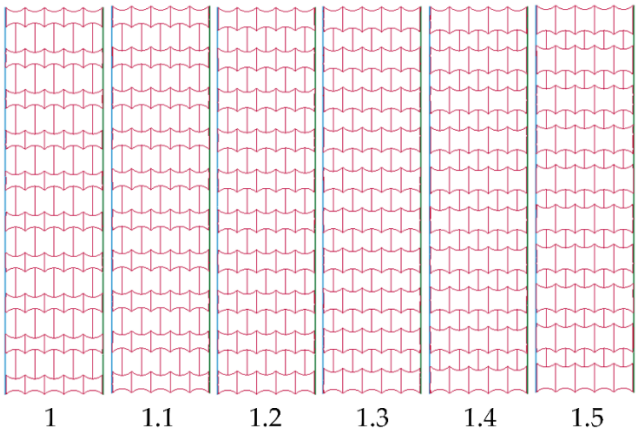

Figure 17. Concave arc honeycomb with different aspect ratio (l/h).

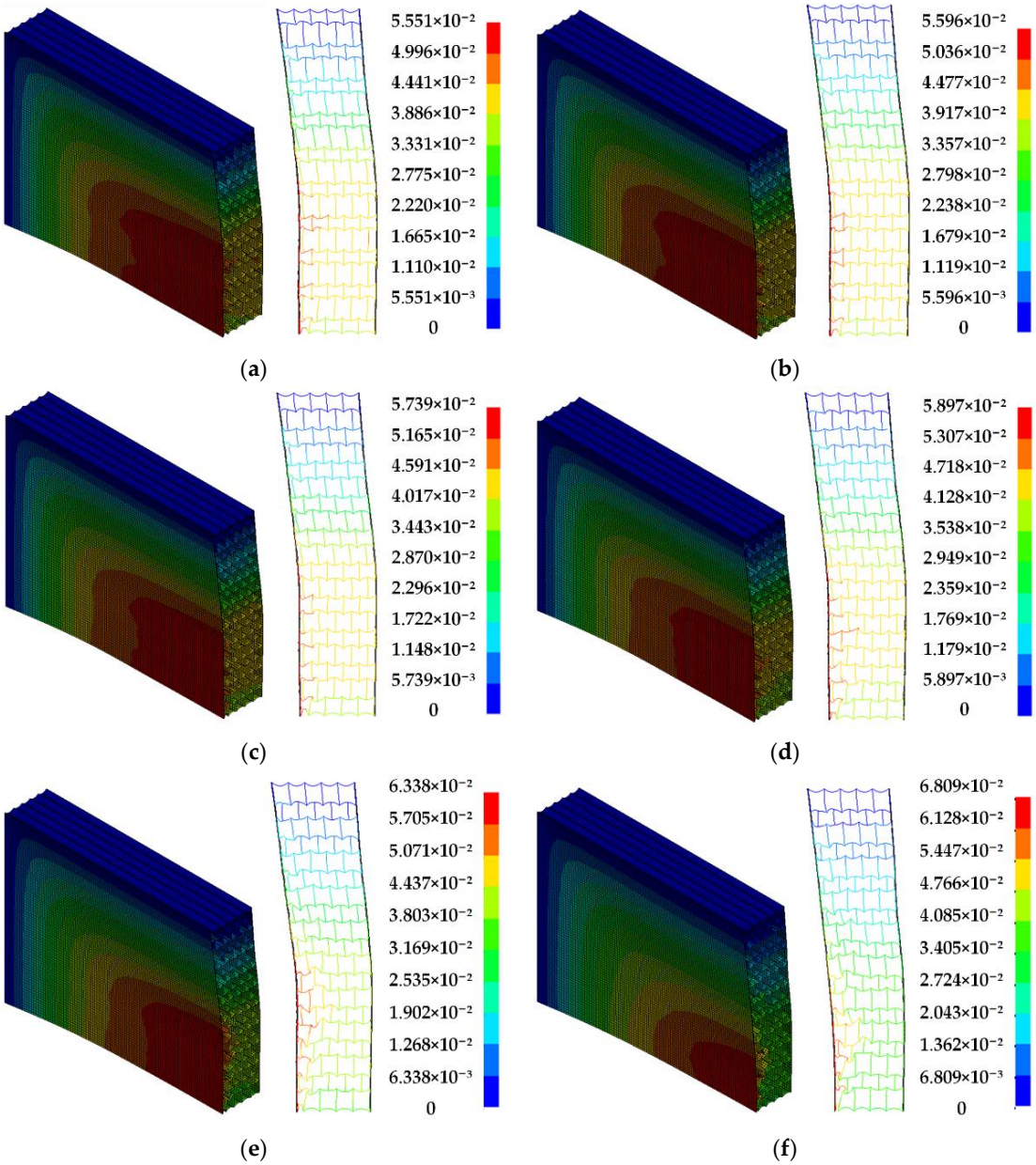

Figure 18. Deformation of different aspect ratio (l/h). (**a**) 1.0; (**b**) 1.1; (**c**) 1.2; (**d**) 1.3; (**e**) 1.4; and (**f**) 1.5.

Figure 19a shows the curve of maximum deformation (δ_{max})–aspect ratio (l/h), from which it can be seen that the maximum deformation δ_{max} of the honeycomb structure gradually increases with the increase of the aspect ratio l/h. The results show that smaller the aspect ratio l/h is, the better performance can be obtained to reduce the amount of the maximum deformation.

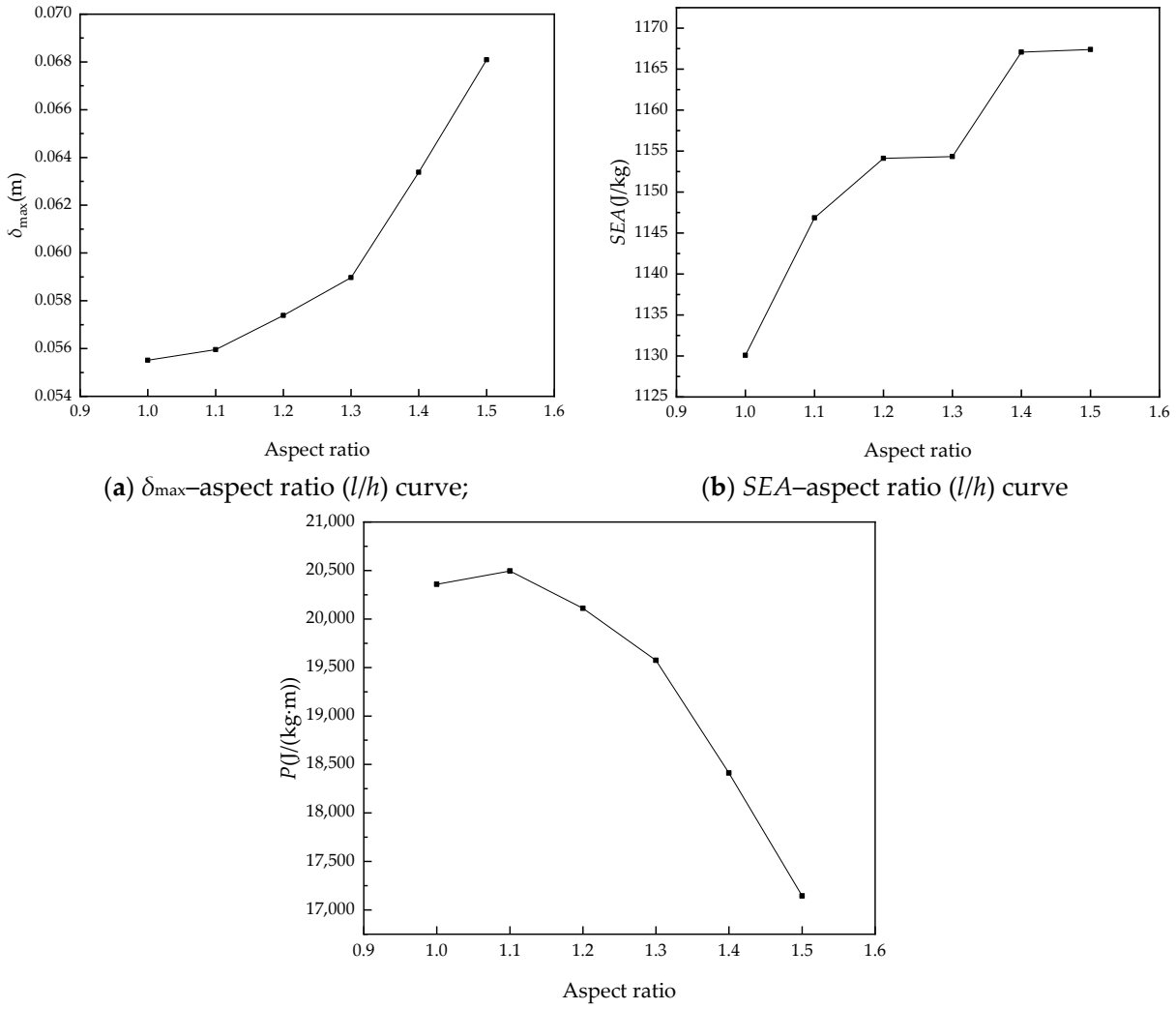

(**a**) δ_{max}–aspect ratio (l/h) curve; (**b**) *SEA*–aspect ratio (l/h) curve

(**c**) *P*–aspect ratio (l/h) curve

Figure 19. The curve of anti-blast index and different aspect ratio (l/h).

Figure 19b shows the *SEA*-θ curve, from which it can be seen that the *SEA* of the sandwich honeycomb structure gradually increases with the increase of the aspect ratio. The results show that the bigger the aspect ratio l/h is, the better performance can be obtained to absorb more energy produced by the blast.

Moreover, the ratio *P*–aspect ratio l/h curve has been plotted and shown in Figure 19c, from which it can be seen that with the increase of the aspect ratio l/h, the ratio *P* increases at first and then decreases. When the aspect ratio l/h= 1.1, the ratio *P* reaches the maximum.

In conclusion, after parameter optimization, the sandwich plate with concave arc honeycomb core when $\theta = 45^{\circ}$ and l/h = 1.1 achieves the best blast-resistance performance, and thus can be regarded as the optimized blast wall-1(OBW-1).

5.2.3. Optimization of Gradient Honeycomb Structures

As discussed in Section 5.2.1, studies proved that the gradient arrangement of the honeycomb cells along the impact direction has a great impact on the impact resistance. In

this section, the concave arc honeycomb structures with positive and negative gradients are constructed to further investigate the influence of gradient direction of the honeycomb core. Specifically, the concave angles of the positive gradient arrangement are set as 35°, 45°, 55°, 65°, and 75°, as shown in Figure 20a. On the contrary, the concave angles of the negative gradient arrangement are set as 75°, 65°, 55°, 45°, and 35°, as shown in Figure 20b.

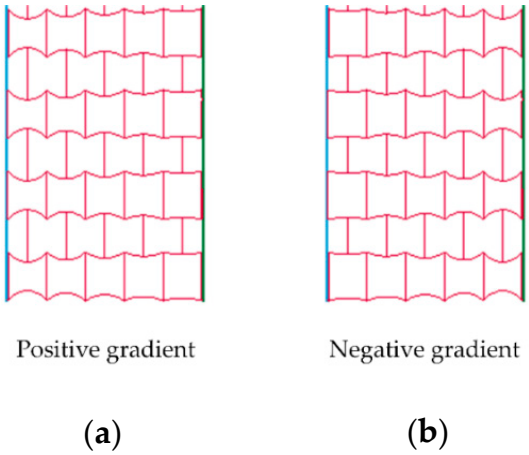

Figure 20. Section of sandwich panel with gradient honeycomb. (**a**) Positive gradient; and (**b**) Negative gradient.

Figure 21a and b shows the deformation modes of the two types of honeycomb structures with different gradients. Although the same deformation mode (i.e., parallelogram bending) appears on the two honeycomb structures, their deformation distributions have a significant difference.

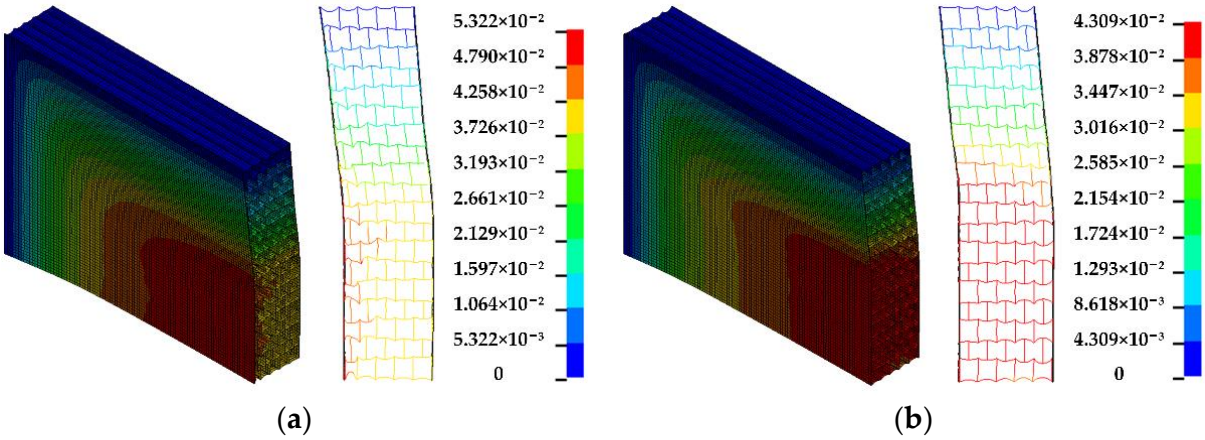

Figure 21. Deformation of different gradient. (**a**) Positive gradient; and (**b**) Negative gradient.

In order to give a detailed deflection history of the positive gradient honeycomb structure and the negative gradient honeycomb structure during blast loading, the cures were plotted in Figure 22a,b. It can be seen from Figure 22a that the deformation of the front face plate and back face plate of the positive gradient honeycomb structure is quite different, which leads to the large compression deformation of the honeycomb core. In contrast, according to Figure 22b, the deformation difference between the front and back plates of the honeycomb structures with negative gradient is not large, which makes the compression deformation of the honeycomb core very small.

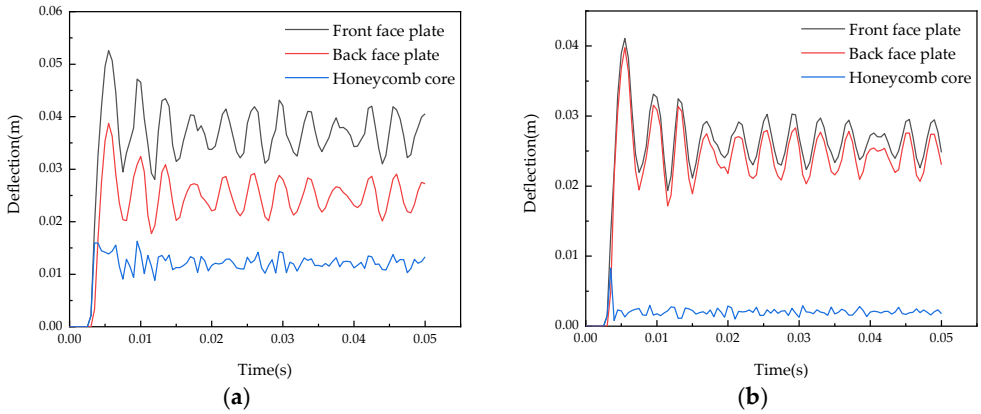

Figure 22. Deflection histories of centre points of face plates and honeycomb core. (**a**) Positive gradient; and (**b**) Negative gradient.

Moreover, compared with Figure 22a,b, it can be seen that the deformation of the front plate with the positive gradient is larger than that of the front plate with the negative gradient. The back face plate deformation of the two gradients is basically the same. According to the comparison results, although the deformation of the positive gradient is larger than that of the negative gradient, the compressive deformation of the honeycomb core layer with the positive gradient is much larger than that of the negative gradient.

The different anti-blast indices (namely $\delta_{\max}$, *SEA*, and *P* of the two types of honeycomb structures with different gradients) have been calculated as listed in Table 7 and compared in Figure 23. Because the value of *P* of the positive gradient honeycomb structure is much larger than that of the negative gradient honeycomb structure we can find that the concave arc honeycomb structure with a positive gradient has better anti-blast performance, which could be regarded as the optimized blast wall-2(OBW-2).

Table 7. The indices of two gradients.

Type	δ_{max} (m)	*SEA* (J/kg)	*P*(J/(kg·m))
Positive gradient	0.0532216	1149.959731	21,607.01164
Negative gradient	0.0430880	768.0236468	17,824.53692

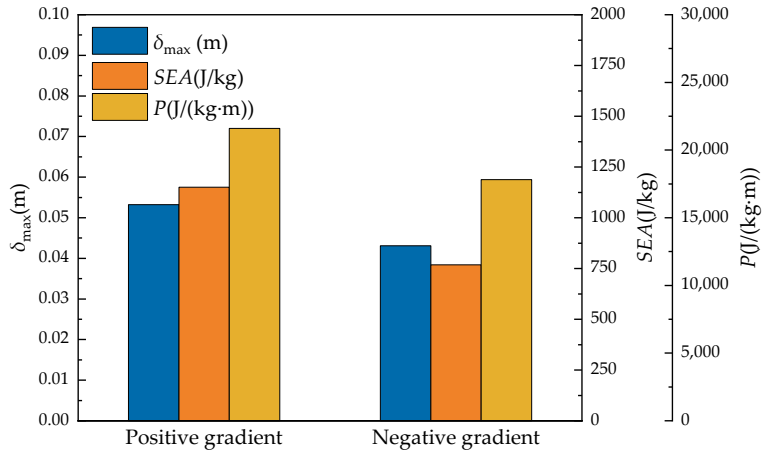

Figure 23. Anti-blast index diagram of two gradients.

5.3. Optimization of Curvature on the Performance of Blast Wall

Conventionally, the blast walls constructed on offshore structures are flat panels. However, some studies [47] have shown that the curved panels generally have better performance under various loadings because they can support the external loads effectively

by virtue of their spatial curvature. In this section, blast walls of different curvatures have been simulated, and the effect of the curvature on the blast resistance has been analyzed through numerical simulation results.

The diagram of the blast wall on the top side of the offshore platform is shown in Figure 24. The size of the blast wall is set as length L = 10 m, height H = 4.4 m, and thickness T = 0.204 m, as shown in Figure 25. The above two kinds of optimized blast wall (i.e., OBW-1 and OBW-2) were selected as the fundamental configuration.

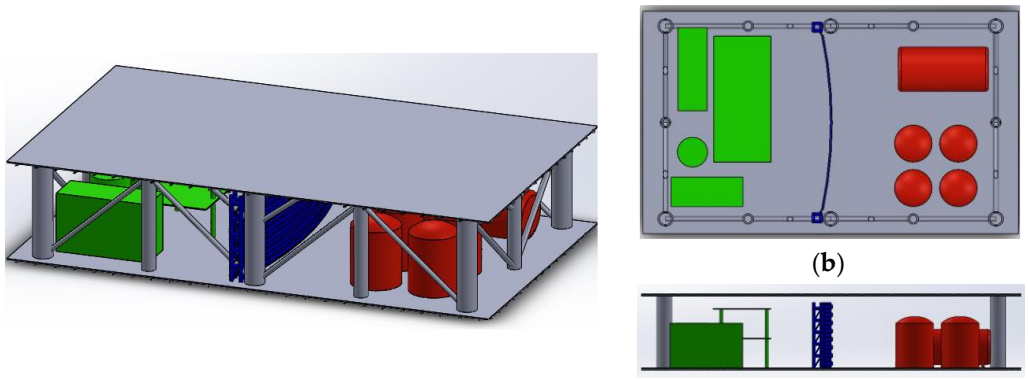

Figure 24. Diagram of the blast walls on offshore platform. (**a**) overall view; (**b**) top view; and (**c**) front view.

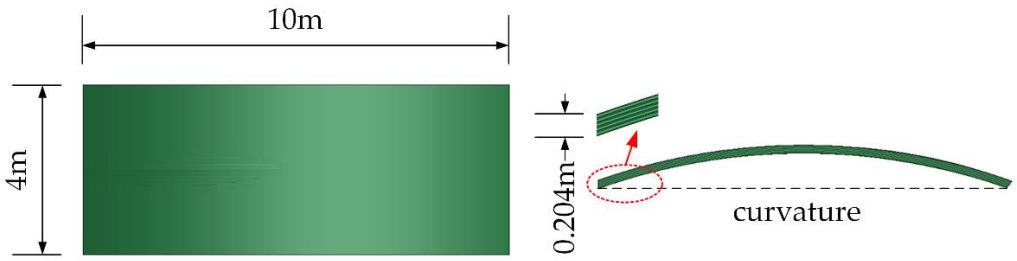

Figure 25. Dimensions of the blast wall.

To investigate the influence of the curvature of the blast wall on the blast resistance, eight different blast walls with curvature including 1/15, 1/20, 1/25, 1/30, 1/35, 1/40, 1/45, and 0, were analyzed. The schematic diagram of blast wall models with different curvatures is shown in Figure 26. The mass of TNT is 100 kg and its position is shown in Figure 27. A fully clamped boundary condition was adopted around the curved blast wall.

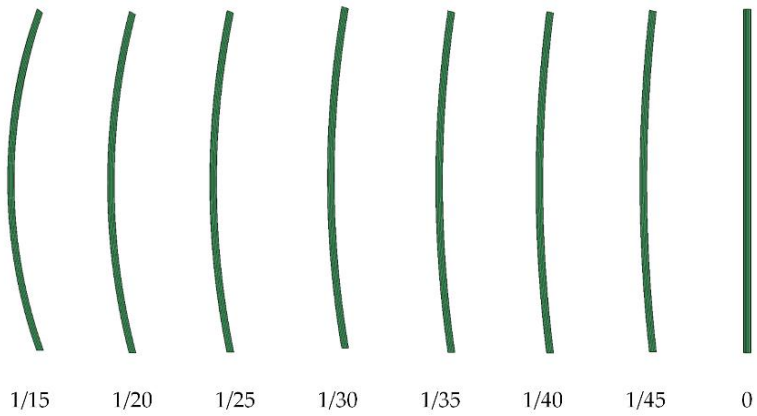

Figure 26. Configurations of blast wall with different curvature (m^{-1}).

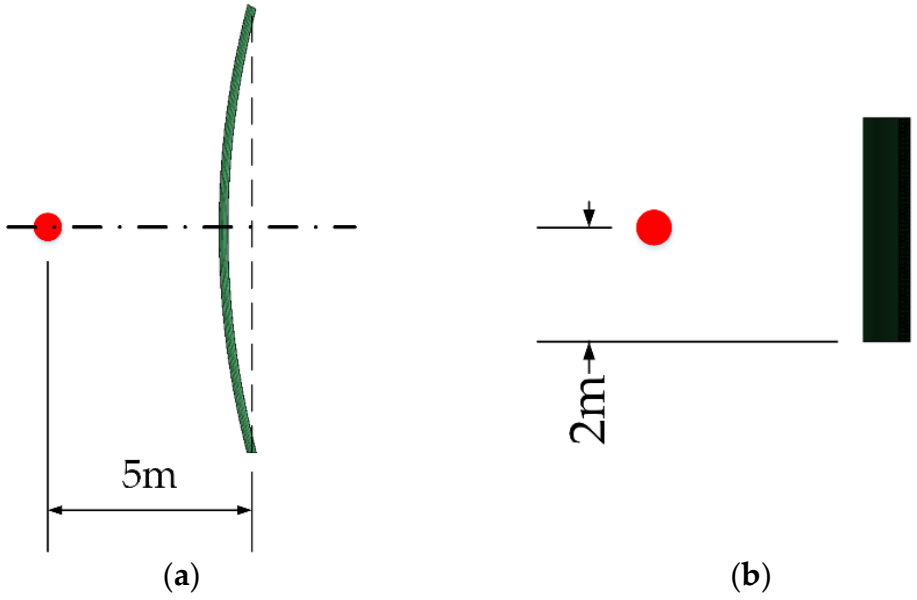

Figure 27. Diagram of TNT position. (**a**) vertical view; and (**b**) left view.

Figure 28a,b shows the δ_{max}–k curve and the TEA–k curve of the global blast wall, respectively. It can be seen that with the increase of curvature k, both the energy absorbed by the blast wall and the maximum deflection gradually increases. In addition, the comprehensive blast resistance index P was calculated according to δ_{max} and TEA, and the result of P shows that when the curvature is 1/20, the value of P is the maximum, which demonstrates that when the curvature is 1/20, the anti-blast performance is the best.

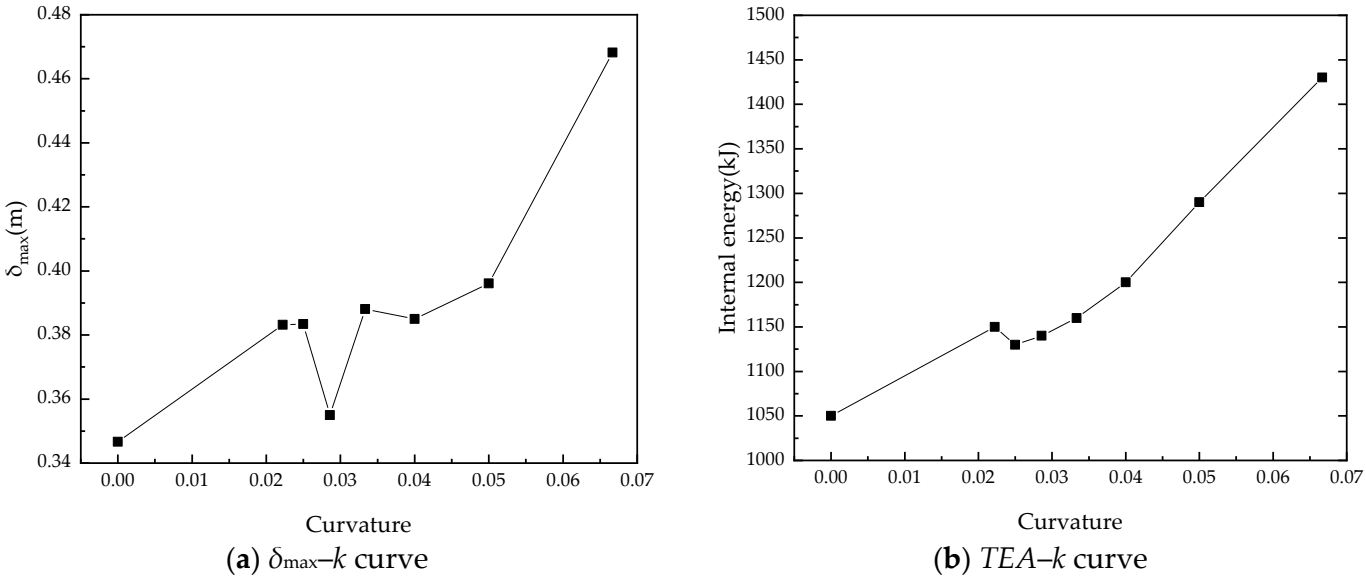

(**a**) δ_{max}–k curve (**b**) TEA–k curve

Figure 28. The curve of anti-blast index and different curvature.

Furthermore, the deformation contour of the blast wall of OBW-1 and OBW-2 with curvature of 1/20 is shown in Figure 29a,b. It can be seen that the maximum deflection δ_{max} of OBW-1 and OBW-2 is 0.3961 m and 0.3915 m, respectively. The result demonstrates that under the same explosive situation, the two kinds of optimized sandwich blast walls of OBW-1 and OBW-2 can achieve equivalent blast-resistance performance.

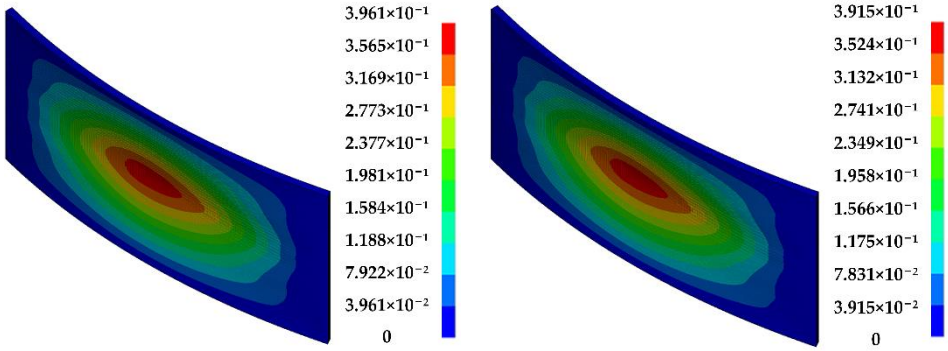

Figure 29. Deformation of blast wall with curvature of 1/20. (**a**) OBW-1; and (**b**) OBW-2.

5.4. Influence of Constraint Conditions

The blast wall may be constructed in different places on the offshore platform with different boundary conditions. In this section, three different types of boundaries (shown in Figure 30) are studied to analyze their influence on the performances of OBW-2.

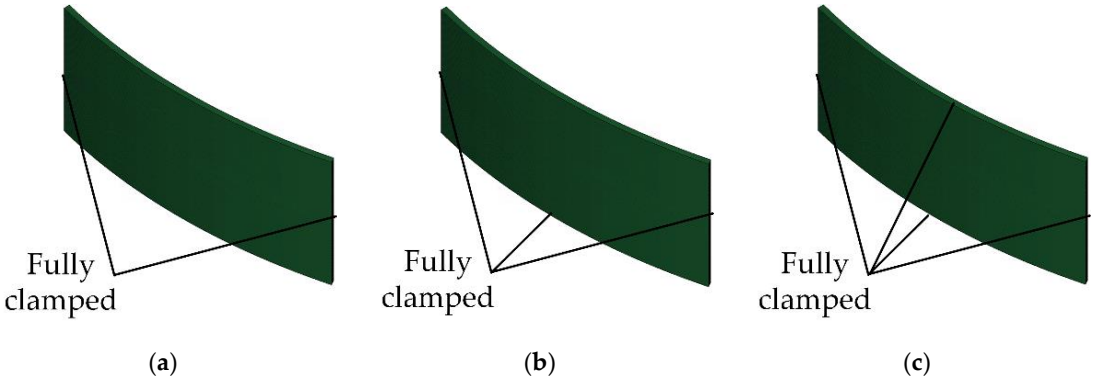

Figure 30. Different boundary conditions. (**a**) Two sides fixed; (**b**) Three sides fixed; (**c**) Four sides fixed.

The deformation contour of the blast wall with different boundary conditions were shown in Figure 31. The different anti-blast indices, namely δ_{max}, *TEA* of different boundary conditions have been calculated as listed in Table 8. It can be seen that the blast wall with four-sided constraints has the smallest deformation, although the explosion-proof wall with three-sided constraints has the largest deformation due to the asymmetry of constraints. By combining the internal energy and the maximum deformation, it can be concluded that the blast wall with four sides fixed has the best anti-blast performance.

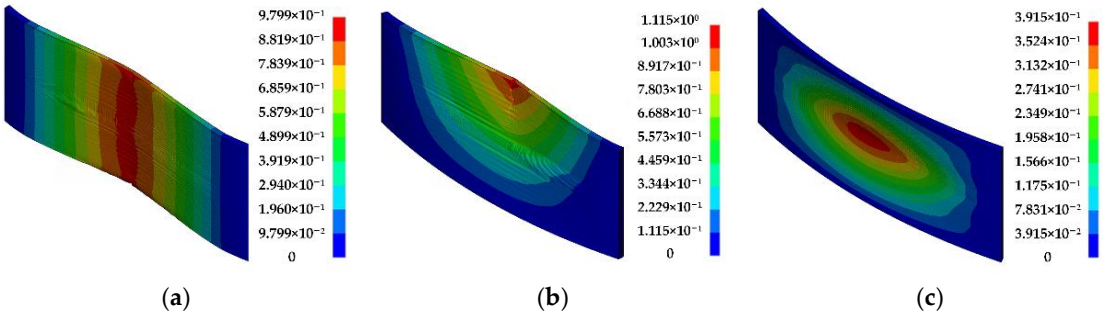

Figure 31. Deformation of blast wall with different boundary conditions. (**a**) Two sides fixed; (**b**) Three sides fixed; and (**c**) Four sides fixed.

Table 8. The indices of different boundary conditions.

Boundary	δ_{max} (m)	*TEA* (J)
Two sides fixed	0.9799	1310
Three sides fixed	1.115	1280
Four sides fixed	0.3915	1250

6. Conclusions

In this paper, the sandwich panel with different types of honeycomb cores including arrow-shaped, concave hexagonal-shaped, and concave arc-shaped cores, were designed and compared to construct an optimized blast wall on an offshore platform. The commercial finite element software ANSYS/LS-DYNA was used to carry out simulations of blast walls under explosive loading based on the CONWEP algorithm. The parametric studies were carried out to examine the effects of the concave angle and the aspect ratio of the unit cell, and also the different gradient rearrangement direction and the curvature of the blast wall. According to different criteria, the blast resistance of the sandwich honeycomb structures was evaluated, and the optimized blast wall of OBW-1 and OBW-2 were obtained. Some important conclusions can be drawn as below:

(1) The sandwich plate with concave arc honeycomb core has the best anti-blast performance compared to that of arrow honeycomb core and concave hexagonal honeycomb core.
(2) The increase of the concave angle could reduce the amount of the maximum deformation of the sandwich concave arc honeycomb structure; however, it will lead to more energy absorption. Comprehensively speaking, when the concave angle is 45°, the best anti-blast performance can be obtained.
(3) The influence of the aspect ratio of the concave arc honeycomb on the blast resistance is smaller, and when the aspect ratio is 1.1, the best anti-blast performance can be obtained.
(4) The concave arc honeycomb structure with positive gradient arrangement has better anti-blast performance than that of the negative gradient.
(5) The curved sandwich honeycomb blast wall shows better energy absorption ability than the flat blast wall, and when the curvature is 1/20 the best anti-blast performance can be obtained. Moreover, the blast wall with four sides fixed has better anti-blast performance.

Author Contributions: Conceptualization, H.L. (Hong Lin) and C.H.; methodology, H.L. (Hong Lin) and C.H.; software, H.L. (Hong Lin), C.H. and L.Y.; validation, H.L. (Haochen Luan), P.H., H.X. and S.Z.; investigation, L.Y. and H.L. (Hong Lin); writing—original draft preparation, H.L. (Hong Lin) and C.H.; writing—review and editing, L.Y. and L.Z.; supervision, H.L. (Hong Lin); project administration, H.L. (Hong Lin) and L.Y.; funding acquisition, H.L. (Hong Lin). All authors have read and agreed to the published version of the manuscript.

Funding: This research was funded by the National Natural Science Foundation of China, grant No. 51879272, No. 52111530036; and the Fundamental Research Funds for the Central Universities, China, grant No. 22CX03022A.

Institutional Review Board Statement: Not applicable.

Informed Consent Statement: Not applicable.

Conflicts of Interest: The authors declare no conflict of interest.

References

1. Det Norske Veritas. *WOAD, Worldwide Offshore Accident Databank*; Det Norske Veritas: Oslo, Norway, 1996.
2. O'Byrne, C. Remembering the Piper Alpha disaster. *Hist Reflect.* **2011**, *37*, 90–104. [CrossRef]
3. National Academy of Engineering and National Research Council. *Macondo Well Deepwater Horizon Blowout: Lessons for Improving Offshore Drilling Safety*; The National Academies Press: Washington, DC, USA, 2012. [CrossRef]
4. Shi, J.; Xie, W.; Huang, X.; Xiao, F.; Usmani, A.S.; Khan, F.; Yin, X.; Chen, G. Real-time natural gas release forecasting by using physics-guided deep learning probability model. *J. Clean. Prod.* **2022**, *368*, 133201. [CrossRef]

5. Det Norske Veritas. *Accident Statistics for Fixed Offshore Units on the UK Continental Shelf 1980–2005*; RR566 Research Report; Health and Safety Executive: Bootle, UK, 2007.
6. Walker, S.; Carney, S.; Fairlie, G.; Louca, L.A. *New Guidance on the Design of Offshore Structures to Resist the Explosion Hazard*; American Society of Mechanical Engineers: New York, NY, USA, 2003.
7. Mostert, F.J. Challenges in blast protection research. *Def. Technol.* **2018**, *14*, 426–432. [CrossRef]
8. Rahman, S.A.; Syed, Z.I.; Kurian, J.V.; Liew, M.S. Structural Response of Offshore Blast Walls under Accidental Explosion. *Adv. Mater. Res.* **2014**, *1043*, 278–282. [CrossRef]
9. Malo, K.A.; Ilstad, H. Response Of Corrugated Steel Walls Due To Pressure Loads. *WIT Trans. Built Environ.* **1970**, *8*, 165–173. [CrossRef]
10. Shi, J.; Zhu, Y.; Chen, G.; Zhang, R.; Guo, Z. Assessment on blast loading resistance capacity of corrugations on offshore cabins based on the P–I model. *Process Saf. Environ. Prot.* **2017**, *105*, 237–249. [CrossRef]
11. Louca, D.; Boh, J.W. *Analysis and Design of Profiled Blast Walls*; HSE (Health Safety Executive): Bootle, UK, 2004.
12. Kang, K.Y.; Choi, K.H.; Choi, J.W.; Yong, H.R.; Lee, J.M. Explosion induced dynamic responses of blast wall on FPSO topside: Blast loading application methods. *Int. J. Nav. Archit. Ocean. Eng.* **2016**, *9*, 135–148. [CrossRef]
13. Syed, Z.I.; Mohamed, O.A.; Rahman, S.A. Non-linear Finite Element Analysis of Offshore Stainless Steel Blast Wall under High Impulsive Pressure Loads. *Procedia Eng.* **2016**, *145*, 1275–1282. [CrossRef]
14. Su, Q.; Zhai, X. Dynamic response of single-layer reticulated shell with explosion-protection wall under blast loading. *Thin-Walled Struct.* **2018**, *127*, 389–401. [CrossRef]
15. Sohn, J.M.; Kim, S.J.; Seo, J.K.; Kim, B.J.; Paik, J.K. Strength assessment of stiffened blast walls in offshore installations under explosions. *Ships Offshore Struct.* **2015**, *11*, 551–560. [CrossRef]
16. Nwankwo, E.; Soleiman Fallah, A.; Langdon, G.S.; Louca, L.A. Inelastic deformation and failure of partially strengthened profiled blast walls. *Eng. Struct.* **2013**, *46*, 671–686. [CrossRef]
17. Gao, Q.; Liao, W.; Wang, L. On the low-velocity impact responses of auxetic double arrowed honeycomb. *Aerosp. Sci. Technol.* **2020**, *98*, 105698. [CrossRef]
18. Wang, Z.G. Recent advances in novel metallic honeycomb structure. *Compos. Part B Eng.* **2019**, *166*, 731–741. [CrossRef]
19. Xiao, D.; Kang, X.; Li, Y.; Wu, W.; Lu, J.; Zhao, G.; Fang, D. Insight into the negative Poisson's ratio effect of metallic auxetic reentrant honeycomb under dynamic compression. *Mater. Sci. Eng. A* **2019**, *763*, 138151. [CrossRef]
20. Luo, F.; Zhang, S.; Yang, D. Anti-Explosion Performance of Composite Blast Wall with an Auxetic Re-Entrant Honeycomb Core for Offshore Platforms. *J. Mar. Sci. Eng.* **2020**, *8*, 182. [CrossRef]
21. Lin, H.; Han, C.; Yang, L.; Karampour, H.; Luan, H.; Han, P.; Xu, H.; Zhang, S. Dynamic Performance and Crashworthiness Assessment of Honeycomb Reinforced Tubular Pipe in the Jacket Platform under Ship Collision. *J. Mar. Sci. Eng.* **2022**, *10*, 1194. [CrossRef]
22. Birman, V.; Kardomateas, G.A. Review of current trends in research and applications of sandwich structures. *Compos. B Eng.* **2018**, 142. [CrossRef]
23. Xiang, X.M.; Lu, G.; Ma, G.W.; Li, X.Y.; Shu, D.W. Blast response of sandwich beams with thin-walled tubes as core. *Eng. Struct.* **2016**, *127*, 40–48. [CrossRef]
24. He, Q.; Ma, D. Parametric study and multi-objective crashworthiness optimisation of reinforced hexagonal hon-eycomb under dynamic loadings. *Int. J. Crashworthiness* **2015**, *20*, 495–509. [CrossRef]
25. Bohara, R.P.; Linforth, S.; Ghazlan, A.; Nguyen, T.; Remennikov, A.; Ngo, T. Performance of an auxetic honey-comb-core sandwich panel under close-in and far-field detonations of high explosive. *Compos. Struct.* **2022**, *280*, 114907. [CrossRef]
26. Li, Z.; Gao, Q.; Yang, S.; Wang, L.; Tang, J. Comparative study of the in-plane uniaxial and biaxial crushing of hexagonal, concave, and mixed honeycombs. *J. Sandw. Struct. Mater.* **2018**, *21*, 1991–2013. [CrossRef]
27. Jin, X.; Wang, Z.; Ning, J.; Xiao, G.; Liu, E.; Shu, X. Dynamic response of sandwich structures with graded auxetic honeycomb cores under blast loading. *Compos. Part B Eng.* **2016**, *106*, 206–217. [CrossRef]
28. Alqwasmi, N.; Tarlochan, F.; Alkhatib, S.E. Study of Mild Steel Sandwich Structure Energy Absorption Performance Subjected to Localized Impulsive Loading. *Materials* **2020**, *13*, 670. [CrossRef]
29. Qi, C.; Remennikov, A.; Pei, L.Z.; Yang, S.; Yu, Z.H.; Ngo, T.D. Impact and close-in blast response of auxetic honey-comb-cored sandwich panels: Experimental tests and numerical simulations. *Compos. Struct.* **2017**, *180*, 161–178. [CrossRef]
30. Imbalzano, G.; Tran, P.; Ngo, T.D.; Lee, P.V.S. A numerical study of auxetic composite panels under blast loadings. *Compos. Struct.* **2016**, *135*, 339–352. [CrossRef]
31. Aslefallah, M.; Abbasbandy, S.; Shivanian, E. Fractional cable problem in the frame of meshless singular boundary method. *Eng. Anal. Bound. Elem.* **2019**, *108*, 124–132. [CrossRef]
32. Aslefallah, M.; Abbasbandy, S.; Shivanian, E. Numerical solution of a modified anomalous diffusion equation with nonlinear source term through meshless singular boundary method. *Eng. Anal. Bound. Elem.* **2019**, *107*, 198–207. [CrossRef]
33. Aslefallah, M.; Shivanian, E. Nonlinear fractional integro-differential reaction-diffusion equation via radial basis functions. *Eur. Phys. J. Plus* **2015**, *130*, 1–9. [CrossRef]
34. Aslefallah, M.; Shivanian, E. An efficient meshless method based on RBFs for the time fractional diffusion-wave equation. *Afr. Mat.* **2018**, *29*, 1203–1214. [CrossRef]

35. Qi, C.; Pei, L.Z.; Remennikov, A.; Yang, S.; Liu, J.; Wang, J.S.; Liao, X.W. Parametric study and optimization of the protect system containing a re-entrant hexagon cored sandwich panel under blast impact. *Compos. Struct.* **2020**, *252*, 112711. [CrossRef]
36. Masters, I.G.; Evans, K.E. Models for the elastic deformation of honeycombs. *Compos. Struct.* **1996**, *35*, 403–422. [CrossRef]
37. Cowper, G.R.; Symonds, P.S. Strain-Hardening and Strain-Rate Effects in the Impact Loading of Cantilever Beams. Ph.D. Thesis, Brown University, Providence RI, USA, 1957.
38. Storheim, M.; Amdahl, J.; Martens, I. On the accuracy of fracture estimation in collision analysis of ship and offshore structures. *Mar. Struct.* **2015**, *44*, 254–287. [CrossRef]
39. Luo, F.; Zhang, S. Flow field pressure analysis of thin explosive acting on corrugated blast wall. *Ocean. Eng.* **2021**, *39*, 135–143. (In Chinese) [CrossRef]
40. Fan, Y.; Wang, Z. Dynamic plastic collapse mechanical model of honeycomb structures out-plane deformation. *J. Beijing Univ. Aeronaut. Astronaut.* **2012**, *38*, 1464–1468. (In Chinese) [CrossRef]
41. Qi, S.; Huang, G.; Zhi, X.; Fan, F. Sensitivity analysis and probability modelling of the structural response of a single-layer reticulated dome subjected to an external blast loading. *Def. Technol.* **2022**. [CrossRef]
42. Slavik, T.P. A coupling of empirical explosive blast loads to ALE air domains in LS-DYNA. *IOP Conf. Ser. Mater. Sci. Eng.* **2010**, *10*, 012146. [CrossRef]
43. Cui, Y.X.; Chen, P.W.; Wang, L.Y.; Wang, D.X.; Xiong, Y.B. Numerical simulation on deformation behavior of multi-layers steel cylindrical structure under internal intense blast loading. *Beijing Ligong Daxue Xuebao/Trans. Beijing Inst. Technol.* **2015**, *35*, 14–17. (In Chinese)
44. Neuberger, A.; Peles, S.; Rittel, D. Scaling the response of circular plates subjected to large and close-range spherical explosions. Part I: Air-blast loading. *Int. J. Impact Eng.* **2007**, *34*, 859–873. [CrossRef]
45. Ni, J. Response Analysis of Single-Layer Reticulated Domes Subjected to External Blast Loading Using CONWEP and Experimental Design. Master's Thesis, Harbin Institute of Technology, Harbin, China, 2012. (In Chinese).
46. Ajdari, A.; Nayeb-Hashemi, H.; Vaziri, A. Dynamic crushing and energy absorption of regular, irregular and functionally graded cellular structure. *Int. J. Solids Struct.* **2011**, *48*, 506–516. [CrossRef]
47. Lan, X.; Feng, S.; Huang, Q.; Zhou, T. A comparative study of blast resistance of cylindrical sandwich panels with aluminum foam and auxetic honeycomb cores. *Aerosp. Sci. Technol.* **2019**, *87*, 37–47. [CrossRef]